Full-Core DEM Simulation of an AVR Pebble Bed: Spatial Characterization of Packing Structure and Spatial Localization of Pebble Wear

Jihwan Lim, Seongmin Hong, Minseop Song*
Department of Nuclear Engineering, Hanyang University, 222 Wangsimni-ro, Seongdong-gu, Seoul, 04761, Republic of Korea
*Corresponding author: hysms@hanyang.ac.kr

***Keywords: Pebble Bed Reactor, AVR, DEM, Pebble Bed Debris**

1. Introduction

Pebble-bed high-temperature gas-cooled reactors (HTGRs) have attracted renewed interest as a near-term Generation-IV technology. China's HTR-PM, the first commercial modular HTGR, entered commercial operation in 2023, and designs such as the Xe-100 are now advancing through licensing. Their appeal lies in strong inherent safety, on-line refueling, and high-temperature heat suitable for both electricity generation and industrial process heat, enabled by robust TRISO-coated fuel.

A distinctive feature of the pebble-bed design is the slow, continuous circulation of fuel pebbles through the core. This motion, combined with pebble-to-pebble and pebble-to-wall friction, generates graphite dust and fragmentation debris [1]. In the German AVR prototype (46 MWth), 50–60 kg of graphite dust was estimated to have been generated over its twenty-year operating life [1], while re-evaluations based on inspections carried out during decommissioning place the total production considerably higher, at 100–200 kg [2]. In either case, friction between circulating pebbles is regarded as a primary generation mechanism [3].

Such dust and fine debris can partially obstruct the narrow interstitial channels between pebbles, causing local flow blockage and coolant maldistribution. Local blockage and flow maldistribution are long-standing concerns for packed beds in general, but in a pebble-bed core they carry a direct safety consequence.

A local reduction of the interstitial flow area degrades local convective cooling and can, in principle, drive localized temperature peaking, or hot spots. The AVR experience illustrates how large such excursions can be: melt-wire monitor pebbles indicated core temperatures more than 200 K above pre-calculated values [4]. A subsequent reactor-physics and thermal-fluid study reported that the stochastic arrangement of neighboring pebbles alone, excluding global core-scale peaking, raises the fuel temperature by less than about 50 K [5]. Reproducing the observed 200 K excursion additionally required a local coolant-flow blockage of about 54%.

Local flow blockage is therefore a physically credible mechanism for large temperature excursions in pebble beds, which in turn makes the spatial distribution of dust generation a quantity of direct safety relevance.

Establishing where debris originates within the core is therefore a prerequisite for any subsequent assessment of localized blockage. Prior discrete-element-method (DEM) studies characterized pebble wear and dust generation in scaled or generic pebble-bed geometries, under the assumption that slow rubbing (sliding) wear dominates while collision-induced wear is neglected [1]. In this study, we present a full-core DEM simulation configured to the AVR core geometry and pebble inventory, in which a drain-and-recycle procedure yields a statistically steady configuration. From this configuration, the spatial packing structure is characterized, and two complementary wear-related measures : an Archard-type sliding wear measure that was used in Rycroft [1] and a collision-dissipation energy measure [6]. Those are introduced to map the spatial distribution of dust-generation propensity across the core. By targeting an actual operated reactor and by accounting for collision-induced wear, this work extends prior scaled, sliding-only analyses and localizes the regions where debris generation is concentrated, providing the spatial basis for subsequent localized-blockage flow analysis.

2. Methods

2.1 DEM Model

Pebble motion was simulated with the open-source DEM code LIGGGHTS [7]. Each pebble is tracked individually in a Lagrangian frame, and its translational and rotational motion is governed by

$$m_i \frac{d\mathbf{v}_i}{dt} = m_i \mathrm{g} + \sum_j \mathrm{F}_{ij} \quad (1)$$

$$I_i \frac{d\omega_i}{dt} = \sum_j T_{ij} \quad (2)$$

where m_i, I_i, v_i, and ω_i are the mass, moment of inertia, translational velocity, and angular velocity of pebble i, g is the gravitational acceleration, and F_{ij} and T_{ij} are the contact force and the resulting torque from each contacting pebble or wall. The contact force was evaluated with a Hookean spring–dashpot model with tangential history and a Coulomb friction limit [6], applied identically to pebble–pebble and pebble–wall contacts. The dimensionless parameters of Rycroft et al. [1] were converted to SI units using a pebble diameter d = 0.060 m, mass m = 0.180 kg, and gravitational acceleration g = 9.81 m/s². Table I lists the resulting input values. The Coulomb friction coefficient μ = 0.35 is the baseline value emphasized in [1], and is consistent with

measured nuclear-graphite friction ranges [8]. Because [1] reported that the accumulated wear per drainage cycle varies by roughly a factor of three over $\mu = 0.2–0.8$, the present maps should be read as spatial distributions at a representative friction level rather than as absolute magnitudes.

Table I. Contact-model parameters

Parameter	Value
Contact model	Hookean with tangential history
Pebble diameter, d	0.060 m
Pebble mass, m	0.180 kg
Normal stiffness, k_n	5.886×10^7 N/m
Tangential stiffness, k_t	1.682×10^7 N/m
Normal damping rate, γ_n	2.022×10^3 s^{-1}
Tangential damping rate, γ_t	1.011×10^3 s^{-1}
Friction coefficient, μ	0.35
Time step, Δt	1.955×10^{-6} s

2.2 Simulation setup

The full bed was generated by inserting pebbles from above and allowing them to settle under gravity [1]. Circulation was then represented by relocating each pebble discharged through the bottom outlet to one of five top inlets at z = 3.60 m. Progress was measured by the cumulative number of recycle events N_{rec}. Because a pebble can be recycled more than once, N_{rec} counts passage events rather than distinct particles.

The first 20,000 recycle events constituted a conditioning stage with the reinsertion velocity $6d/\tau = 4.60$ m/s adopted in [1], where $\tau = \sqrt{d/g} = 0.0782$ s. A further 10,000 events were run at $V_z = -1.00$ m/s as the production stage. In the actual reactor, pebbles are reinserted under gravity alone. A zero-velocity reinsertion was therefore attempted first so as to reproduce this condition, but it produced persistent jamming above the free surface and the circulation did not reach a statistically steady state. A reinsertion velocity of −1.00 m/s was the lowest value that maintained stable circulation, and it was adopted for the production stage in order to remain as close as practicable to the gravity-driven reinsertion of the actual reactor. Packing statistics and both wear-related measures reported below were accumulated only during this production stage. The recycle counts are numerical sampling controls and should not be interpreted as the AVR operating throughout.

Table II. Drainage–recycle schedule

Stage	Events	Reinsertion V_z
Conditioning	0–20,000	−4.60 m/s
Production	20,000–30,000	−1.00 m/s

2.3 AVR Geometry

The simplified AVR-derived geometry is shown in Fig. 1. The vessel consists of a cylindrical region with a radius of 1.50 m, a lower cone inclined at 30° to the horizontal, and a central outlet chute with a radius of 0.25 m. The z coordinate is measured from the bottom of the outlet chute, so that the chute, the cone, and the cylindrical region occupy $0 \le z < 0.18$ m, $0.18 \le z < 0.90$ m, and $z \ge 0.90$ m, respectively. Five top inlets were used: one central inlet and four outer inlets placed at a radius of 1.20 m. The principal dimensions and the 100,000-pebble inventory follow the AVR data compiled by Cogliati et al. [2]. The outlet-chute length was assigned a nominal value because it is not reported consistently. Control-rod noses, wall dimples, and other internal details were also omitted, and the vessel walls were modeled as smooth.

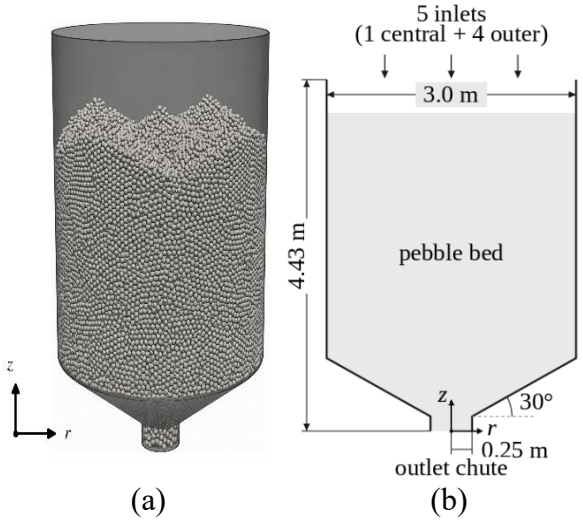


Fig. 1. Schematic of DEM packing (a) and AVR geometry (b)

2.4 Spatial structure characterization

The volume-weighted porosity of the settled bulk bed ($0.18 < z < 3.0$ m) was monitored every 500 recycle events and reached a stable condition after approximately 15,000 events. During the production stage, its mean value was 0.4077, with a relative peak-to-peak variation of only 0.272%. Spatial packing statistics were then averaged over 200 snapshots sampled during the production interval. The volume of each pebble lying inside a sampling region was evaluated directly instead of assigning an entire pebble according to its center. Porosity was evaluated in the cone, lower cylinder, and upper cylinder ($0.18 \le z < 0.90$ m, $0.90 \le z < 1.50$ m, and $1.50 \le z < 3.00$ m) and as a near-wall radial profile in the fixed-radius cylindrical section.

The flow structure was represented by a relative downward velocity. The circumferential mean

downward velocity in each 60 mm r–z cell was divided by a single reference value:

$$U_{\mathrm{rel}}(r,z) = \frac{\bar{u}(r,z)}{\bar{u}_{\mathrm{ref}}} \qquad (3)$$

Here $\bar{u}_{\mathrm{ref}}$ is the particle-weighted mean downward velocity of the whole analyzed domain, 0 < z < 3.0m. The same reference is applied to every cell, so $U_{\mathrm{rel}} = 1$ denotes the domain-mean velocity and the map is directly comparable across the entire domain. A logarithmic colour scale is used. Cells with $z \geq 3.0\,\mathrm{m}$ were excluded; this cut-off lies below the free surface of the settled bed and removes the reinsertion and free-fall region.

2.5 Wear-related measures

Two time-integrated measures were used to locate mechanical loading potentially associated with debris generation. They do not predict an absolute worn mass because conversion to graphite removal requires material-dependent wear coefficients that are not established for the present reactor conditions.

Following Rycroft et al. [1], the Archard-type sliding wear measure accumulates the irreversible tangential correction Δs_t applied when the trial tangential force exceeds the Coulomb limit:

$$W_{\mathrm{slide}} = |F_n||\Delta s_t| \quad [\mathrm{N\,m}] \qquad (4)$$

The collision-dissipation energy measure accumulates the energy dissipated by the normal dashpot [6] while a contact persists:

$$W_{\mathrm{coll}} = c_n v_n^2 \Delta t, \quad c_n = m_{\mathrm{eff}}\gamma_n \quad [\mathrm{J}] \qquad (5)$$

Here, v_n is the relative normal velocity, γ_n is the normal damping rate, and $m_{\mathrm{eff}} = m_i m_j/(m_i + m_j)$ is the effective mass, which equals $m/2$ (0.090 kg) for pebble–pebble contacts and m (0.180 kg) for pebble–wall contacts. Both pebble–pebble and pebble–wall contributions were accumulated.

Each contact evaluation was assigned to a 60 mm axisymmetric r–z cell using r = $\sqrt{x^2 + y^2}$ and all circumferential contributions in that annulus were accumulated over every time step of the production stage to give the cell total $W_{m,ij}$. Because outer cells represent larger three-dimensional volumes than inner cells, each cumulative cell value was divided by its exact annular volume:

$$V_{ij} = \pi(r_{\mathrm{out}}^2 - r_{\mathrm{in}}^2)\Delta z \qquad (6)$$

$$S_{m,ij} = \frac{W_{m,ij}}{V_{ij}} \qquad (7)$$

Thus, $S_{m,ij}$ is the cumulative wear-related density over the 10,000-event production stage. The maps show the full-circumference result on the half-domain 0 ≤ r ≤ 1.5 m. Only 0 ≤ z < 3.0 m and cells inside the vessel profile were retained. The upper limit excludes the reinsertion region, where the contact statistics reflect the prescribed insertion velocity rather than the bulk flow; a comparable wear cut-off height was used in [1]. Independent logarithmic colour scales were used.

3. Results and Discussion

3.1 Packing structure

The time-averaged porosities were 0.422 in the conical section, 0.412 in the lower cylinder, and 0.403 in the upper cylinder. Fig. 2 shows the height-averaged radial profile in the cylindrical section. The wall-adjacent bin had a porosity of 0.886, followed by a minimum of 0.231 at approximately $0.55D_p$ and a maximum of 0.621 near $1.05D_p$. These damped oscillations reflect wall-induced layering of monodisperse pebbles.

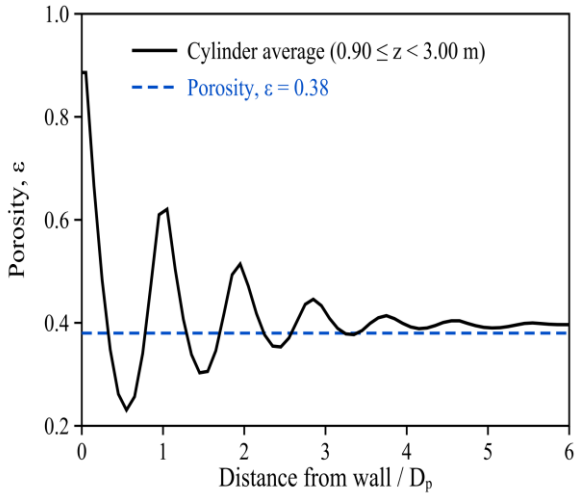


Fig. 2. Time-averaged radial porosity profile in the cylindrical bed (0.90 ≤ z < 3.00 m). Distance is normalized by D_p = 0.060 m; the dashed line marks ε = 0.38.

In Fig. 2. , the wall-adjacent value of 0.886 is a volume average over the first $0.1D_p$ thick layer next to the wall, rather than the exact value at the wall. The oscillation amplitude decreased progressively with distance from the wall. Over $4–6D_p$, the porosity ranged from 0.389 to 0.404, with a mean of 0.396. Wall-induced ordering is therefore concentrated mainly within the first approximately $3D_p$, while a nearly uniform, bulk-like structure is recovered from approximately $4D_p$. The dashed ε = 0.38 line is a commonly quoted bulk value; the far-field value of the present bed is slightly higher.

3.2 Pebble flow structure

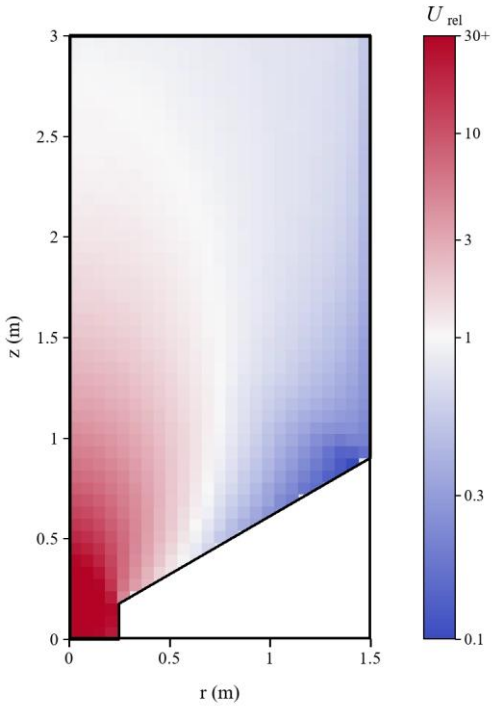


Fig. 3. Spatial distribution of the relative downward pebble velocity, normalized by the domain mean..

Fig. 3. shows the spatial distribution of the relative downward pebble velocity, U_{rel}, defined in Eq. (3).

In the cylindrical section ($0.90 \leq z < 3.00$ m), the pebbles moved faster in the central region and slower near the wall. Mean U_{rel} was approximately 1.61 in the central region ($0 \leq r < 0.30$ m) and 0.45 in the near-wall region ($1.38 \leq r \leq 1.50$ m) . The minimum velocity occurred near the junction between the cylindrical wall and the cone, where U_{rel} decreased to approximately 0.10.

In the conical section, the downward velocity increased as the pebble flow converged toward the discharge chute. The mean U_{rel}in the outlet chute was approximately 30.6, indicating a significant acceleration compared to that in the cylindrical bed. Consequently, the largest spatial variation in downward velocity was observed in the lower converging region.

3.3 Wear-related measure distributions

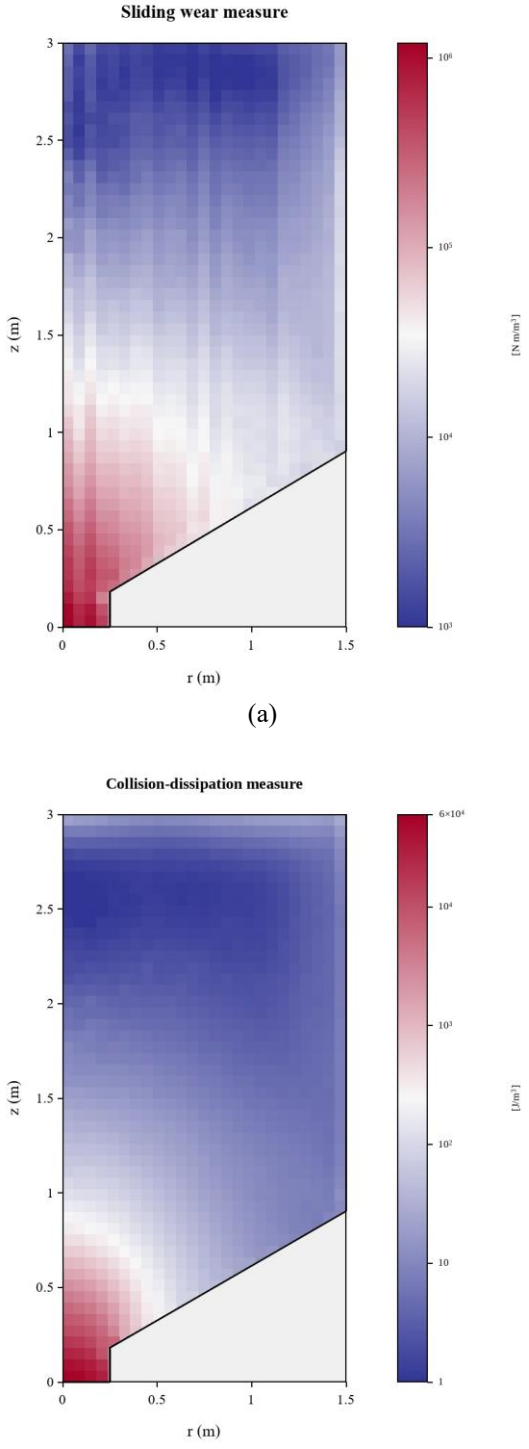


Fig. 4. Spatial distributions of the cumulative (a) sliding wear measure and (b) collision-dissipation measure

Fig. 4 shows the spatial distributions and Table III gives the zone-resolved distribution. About half of the sliding wear measure is contained in the outlet chute and the cone, while the other half remains distributed over the

lower and upper cylinder. The collision-dissipation measure is far more localized, with more than 90% contained in the outlet chute and the cone alone.

The difference reflects what each measure requires. The collision-dissipation measure depends on the normal relative velocity, which is generated mainly where pebbles leave the bed and the remaining pebbles rearrange into the vacated space. This rearrangement is confined to the discharge region, so the spatial influence of collisional dissipation is narrow. The sliding wear measure additionally requires a loaded contact, and the velocity difference between the fast central flow and the slow near-wall layer seen in Fig. 3 provides relative sliding throughout the cylindrical bed. A substantial part of the sliding wear measure is therefore retained outside the converging region.

Table III. Zone-resolved distribution of the cumulative wear-related measures ($0 \le z < 3.0$ m)

Region	z (m)	Volume (%)	Sliding wear (%)	Collision-dissipation (%)
Outlet chute	0–0.18	0.2	6.3	54.9
Cone	0.18–0.90	12.0	42.6	38.6
Lower cylinder	0.90–1.50	25.0	29.7	3.8
Upper cylinder	1.50–3.00	62.7	21.4	2.8

4. Conclusions

A full-core DEM simulation of an AVR-derived pebble bed containing 100,000 pebbles was used to characterize packing, relative flow, and two wear-related measure fields. After conditioning, the bulk porosity was statistically stationary, and the settled bed had zone-averaged porosities of 0.403–0.422. Pronounced near-wall layering decayed within approximately $3D_p$, with a bulk-like profile recovered from about $4D_p$. The relative flow field exhibited a center-fast, wall-slow structure that narrowed toward the outlet.

Both wear-related measure densities were highest in the converging lower bed. About half of the sliding wear measure was retained in the cylindrical section, whereas more than 90% of the collision-dissipation measure was confined to the cone and the outlet chute.

These fields are spatial indicators rather than predictions of worn mass. They identify the source locations required for a subsequent debris-transport calculation, the results of which will be imposed as a local porosity reduction in a CFD analysis of the interstitial coolant flow, allowing the degree of local blockage and the associated temperature peaking to be quantified.

ACKNOWLEDGEMENT

This work is financially supported by the Korea Institute of Energy Technology Evaluation and Planning (KETEP) grant funded by the Ministry of Trade, Industry and Energy (MOTIE) of the Republic of Korea (No. RS-2024-00398867) and the National Research Foundation of Korea (NRF) grant funded by the Korea government (MSIT) (No. RS-2025-02310831).

REFERENCES

[1] C. H. Rycroft, A. Dehbi, T. Lind, S. Güntay, "Granular flow in pebble-bed nuclear reactors: Scaling, dust generation, and stress," *Nuclear Engineering and Design*, Vol. 265, pp. 69–84, 2013.

[2] J. J. Cogliati, A. M. Ougouag, J. Ortensi, "Survey of dust production in pebble bed reactor cores," *Nuclear Engineering and Design*, Vol. 241, No. 6, pp. 2364–2369, 2011.

[3] P. W. Humrickhouse, "HTGR Dust Safety Issues and Needs for Research and Development," Idaho National Laboratory, INL/EXT-11-21097, 2011.

[4] R. Moormann, "AVR prototype pebble bed reactor: a safety re-evaluation of its operation and consequences for future reactors," *Kerntechnik*, Vol. 74, No. 1–2, pp. 8–21, 2009.

[5] V. Sobes, B. Forget, A. Kadak, "Individual pebble temperature peaking factor due to local pebble arrangement in a pebble bed reactor core," *Nuclear Engineering and Design*, Vol. 241, No. 1, pp. 124–133, 2011.

[6] L. E. Silbert, D. Ertaş, G. S. Grest, T. C. Halsey, D. Levine, S. J. Plimpton, "Granular flow down an inclined plane: Bagnold scaling and rheology," *Physical Review* E, Vol. 64, No. 5, p. 051302, 2001.

[7] C. Kloss, C. Goniva, A. Hager, S. Amberger, S. Pirker, "Models, algorithms and validation for open source DEM and CFD-DEM," *Progress in Computational Fluid Dynamics*, Vol. 12, No. 2–3, pp. 140–152, 2012.

[8] X. Luo, X. Li, S. Yu, "Nuclear graphite friction properties and the influence of friction properties on the pebble bed," *Nuclear Engineering and Design*, Vol. 240, No.10, pp. 2674–2681, 2010.